Materials Research. 2016; 19(5): 1155-1161
DOI: http://dx.doi.org/10.1590/1980-5373-MR-2016-0252

Novel $Gd(OH)_3$, GdOOH and Gd_2O_3 Nanorods: Microwave-Assisted Hydrothermal Synthesis and Optical Properties

Maciel Salomão de Almeida[a], Maria Aparecida Bezerra dos Santos[a], Rosana de Fátima Gonçalves[b]*, Maria Rita de Cássia Santos[a], Ana Paula de Azevedo Marques[b], Elson Longo[c], Felipe de Almeida La Porta[d], Ivo Mateus Pinatti[e], Maya Dayana Penha Silva[e], Mario Junior Godinho[a,e]

[a]Unidade Acadêmica Especial de Física e Química – Regional Catalão, Universidade Federal de Goiás – UFG, 75.704–020, Catalão, GO, Brazil
[b]Universidade Federal de São Paulo – UNIFESP, Rua Prof. Artur Riedel, 275, CEP 09972-270, Diadema, SP, Brazil
[c]Laboratório Interdisciplinar de Eletroquímica e Cerâmica – LIEC, Instituto de Química – IQ, Universidade Estadual Paulista, P.O. Box 355, 14801-907, Araraquara, SP, Brazil
[d]Universidade Tecnológica Federal do Paraná – UTFP, 86036-370, Londrina, Brazil
[e]Universidade Federal de São Carlos – UFSCar, Rod. Washington Luiz, Km. 235, CEP 13.565-905, São Carlos, SP, Brazil

Received: March 27, 2016; Revised: June 28, 2016; Accepted: August 11, 2016

We present a study of the controlled synthesis and optical properties of single-crystals $Gd(OH)_3$, GdOOH and Gd_2O_3 nanorods. In this work, $Gd(OH)_3$ nanorods were synthesized by a simple and fast microwave-assisted hydrothermal method. This process combined with the thermal decomposition oxidation of $Gd(OH)_3$ nanorods as precursors enabled the preparation of single-crystalline GdOOH and Gd_2O_3 structures with well-defined morphology at low temperatures. The crystal structure dependence on the optical properties was investigated. We observed a green shift effect on the photoluminescence (PL) emission spectra from $Gd(OH)_3$ to Gd_2O_3 nanorods, which can be attributed to different types of surface defects, as well as intrinsic properties that contribute significantly to the modified PL behavior.

Keywords: *$Gd(OH)_3$, GdOOH, Gd_2O_3, nanorods*

1. Introduction

Nowadays, rare earth hydroxide/oxide nanomaterials have received special attention because of their excellent physical and chemical properties, which provide a wide variety of applications in the nanotechnology field[1-6]. Among various types of rare earth hydroxide/oxide materials, gadolinium hydroxide ($Gd(OH)_3$), gadolinium oxyhydroxide (GdOOH) and gadolinium oxide (Gd_2O_3) exhibit important functional properties that depend on the structure. Gadolinium oxyhydroxide is a stable phase obtained by the thermal dehydration of gadolinium hydroxide and has a simple layered structure. So, these materials have been investigated as promising candidates in the field of high throughput luminescent devices, catalysis and other functional devices based on their excellent electronic, optical and physicochemical responses arising from 4*f* electrons[5-7].

Despite the recent improvements, few studies have been reported concerning the synthesis control of new rare earth hydroxide/oxide nanomaterials. Therefore, more studies leading to the development of new synthetic strategies that allow a superior control in the processing of such materials are needed and this remains a highly challenging field.

Some methods are reported in the literature to obtain well defined $Gd(OH)_3$, GdOOH and Gd_2O_3 nanostructures such as electrochemical route, microwave, sol-gel synthesis, combustion, solid state reaction, and polyol method[3-8]. However, most of these methods require long processing times due to slow reaction kinetics. Therefore, the microwave-assisted hydrothermal (MAH) method has shown numerous advantages such as the use of an environmentally friendly solvent (water) and low processing temperatures (≤200 °C). This method provides a simple and fast approach for the large-scale production of new emergent complex functional materials. In addition, it also enables the shape-controlled synthesis of micro- and/or nanomaterials at a lower cost, for their industrial exploitation with unprecedented capabilities in the new technologies[9-14].

Herein, we report a facile and simple, low-temperature synthesis of single-crystalline $Gd(OH)_3$, GdOOH and Gd_2O_3 nanorods obtained by the MAH method combined with thermal decomposition oxidation process. These microcrystals were structurally characterized by different techniques and the optical properties of the crystal structures obtained were investigated using ultraviolet-visible (UV-vis) diffuse reflectance spectroscopy and photoluminescence (PL) measurements at room temperature. Moreover, this

* e-mail: rosanaf.gon@gmail.com

paper discuss the electronic effects in order to establishes a close correlation between the structure and properties for the single-crystalline $Gd(OH)_3$, GdOOH and Gd_2O_3 nanorods.

2. Experimental

The $Gd(OH)_3$ nanorods were prepared using a MAH method. Initially, a solution of Gd^{3+} was prepared by dissolving gadolinium nitrate (99.9%, Aldrich) in distilled water to obtain a concentration of 0.1 mol L^{-1}. Under magnetic stirring, an ammonium hydroxide solution was added dropwise to complete the precipitation (final pH = 10), resulting in a white gel. In the second stage, the white gel is dispersed in water and the aqueous precursor solution was transferred into a Teflon autoclave, which was properly sealed and placed inside a domestic MAH system (2.45 GHz, maximum power of 800 W). MAH processing was performed at 130ºC under a constant pressure of approximately 3 bar for 20 min. After the hydrothermal treatment, the dispersed powder was centrifuged and washed with distilled water until the residual ions in the solution were eliminated. The resulting product was dried at room temperature for 24 h.

GdOOH and Gd_2O_3 nanocrystals were obtained by a thermal decomposition oxidation process using the $Gd(OH)_3$ nanocrystals prepared by the MAH synthesis as precursors. In both cases, the heating rate was fixed at 3ºC min^{-1} using a conventional furnace (ambient air), obtaining a white powder. The $Gd(OH)_3$ was calcined at either 380 or 600ºC for 60 min, depending on the type of nanocrystals envisaged (GdOOH or Gd_2O_3, respectively).

XRD measurements were performed on a Shimadzu XRD 6100 with CuK_α radiation (40 kV, 30 mA, $\lambda = 0.15418$ nm). The diffraction pattern was measured between 5º and 75º with a step size of 2º s^{-1}. The size and morphologies were characterized by FE-SEM (FEG-VP Zeiss Supra 35) and high-resolution transmission electron microscopy (HRTEM, Jeol, JEM-2100). The thermogravimetric (TG) analyses were carried out with a Netzsch-409 STA simultaneous thermogravimetric-differential thermal analysis (TG-DTA) apparatus with a heating rate of 10ºC min^{-1} under flowing air. DR spectra were produced using a Varian Cary 5G(USA) spectrophotometer in diffuse reflectance mode. PL spectra were collected with a thermal Jarrel-Ash Mono Spec Monochromator and a Hamamatsu R446 photomultiplier. A krypton ion laser (Coherent Innova) with an excitation wavelength of 350.7 nm was used, with the laser nominal output kept at 200 mW. All measurements were performed at room temperature.

3. Results and discussion

Figure 1(a) presents the XRD patterns of the as-prepared $Gd(OH)_3$ powder and $Gd(OH)_3$ powder after the MAH treatment. For the sample processed with the MAH method,

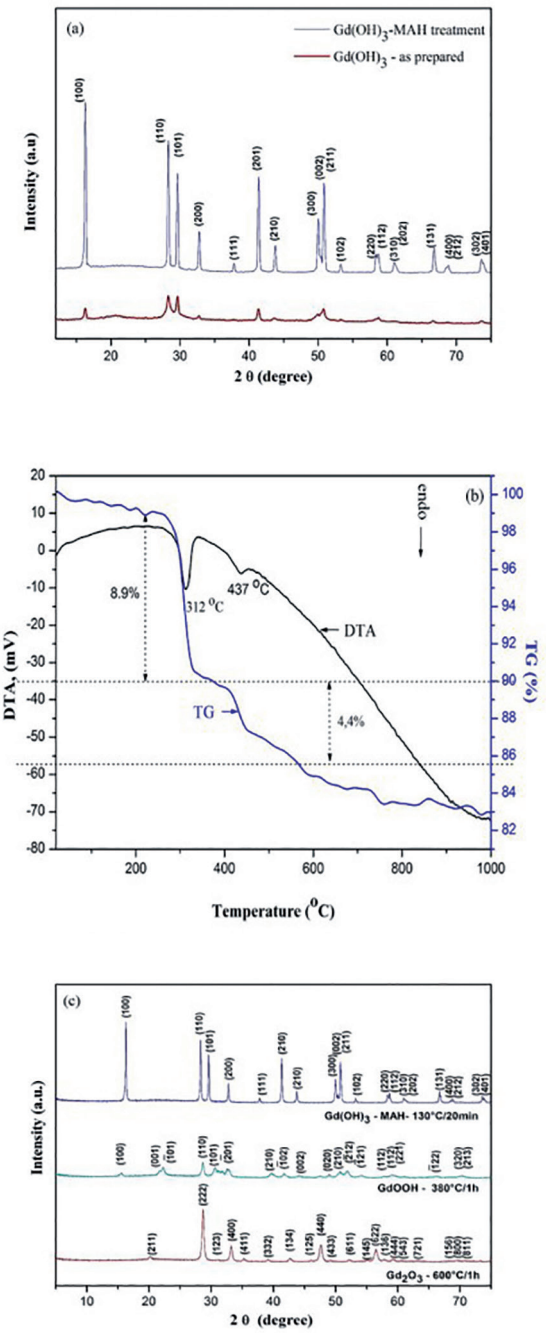

Figure 1: XRD patterns of (a) as-prepared $Gd(OH)_3$ with and without the use of MAH treatment (b) TG/DTA curves of the $Gd(OH)_3$ prepared by the MAH method (c) XRD patterns of the $Gd(OH)_3$, GdOOH and Gd_2O_3 nanocrystals.

all the diffraction peaks can be perfectly indexed to the hexagonal structure of the $Gd(OH)_3$ powders, in agreement with the respective Joint Committee on Powder Diffraction Standard (JCPDS) cards nº 083-2037. No impurities were detected, which in turn reveals the important role of the MAH method in the processing and characteristics of the obtained $Gd(OH)_3$ powders. Moreover, this method enabled

the synthesis of highly crystalline products featuring a long-range-ordered single-phase (Figure 1(a)).

Figure 1(b) shows the TG/DTA curve for the $Gd(OH)_3$ sample prepared by the MAH method at 130ºC for 20 min. Our measurements reveal the presence of two major stages with rapid weight losses at about 312 and 437ºC (8.9 and 4.4%, respectively), suggesting the existence of an intermediate phase during the thermal conversion process of $Gd(OH)_3$ to Gd_2O_3. Interestingly, the total weight loss is in agreement with the theoretical value found for the complete dehydration of $Gd(OH)_3$ to produce Gd_2O_3 (13.3%), as previously reported[15,16]. The thermal dehydration process of the $Gd(OH)_3$ and subsequent conversion to Gd_2O_3 observed in the Figure 1(b) is supposed to occur in two steps, as summarized by equations (1) and (2).

$$Gd(OH)_3 \longrightarrow GdOOH + H_2O \quad (1)$$

$$2GdOOH \longrightarrow Gd_2O_3 + H_2O \quad (2)$$

In this study, a two-step approach was used to synthesize the GdOOH and Gd_2O_3 powders at optimal conditions. Based on these results, we chose two different temperatures (380 and 600ºC) to produce GdOOH and Gd_2O_3 powders, respectively, using a thermal decomposition process of the $Gd(OH)_3$ powder obtained previously by the MAH method.

As shown in Figure 1(c), all the diffraction peaks can be perfectly indexed to the hexagonal structure of $Gd(OH)_3$ (JCPDS 083-2037), monoclinic structure of GdOOH (JCPDS 075-3267) and cubic structure of Gd_2O_3 (JCPDS 072-6362), respectively[16-19]. However, the peak widths for Gd_2O_3 are relatively broader than those observed in the XRD patterns of GdOOH and $Gd(OH)_3$, suggesting a smaller crystallite size. The crystallite sizes were estimated using the Scherrer equation[17], obtaining 34.9, 19.9 and 15.7 nm for $Gd(OH)_3$, GdOOH and Gd_2O_3, respectively. Therefore, the average crystallite size decreases as a function of the dehydration process. This behavior is explained by the dehydration process during the phase change, as well as the synthesis method employed, which facilitates the preparation of materials with small particle sizes.

Figure 2 shows the representations of the unit cells for the hexagonal $Gd(OH)_3$ structure with a *P63/m* space group, the monoclinic GdOOH structure with a *P121/m1* space group, and the cubic Gd_2O_3 structure with an *Ia-3* space group[18-20]. VESTA program was used for the construction and visualization of these three models[21]. In this study, the most important difference between the crystalline phases is the coordination of the gadolinium ions in the ideal crystal structure. The hexagonal $Gd(OH)_3$ structure has a nine-coordination complex with $[Gd(OH)_9]$ clusters, the monoclinic GdOOH structure has a seven-coordination complex with $[GdO(OH)_7]$ clusters, and the cubic Gd_2O_3 structure has a six-coordination complex with $[GdO_6]$ clusters. It is well known that lanthanide ions have a wide variety of coordination

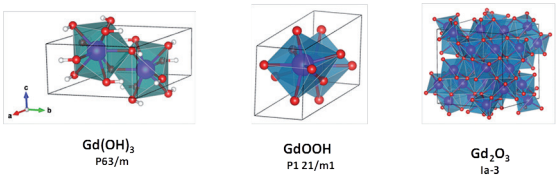

Figure 2: Schematic representation of the unit cells corresponding to the hexagonal, monoclinic and cubic structure of the materials.

environments, and in general tend to form complex clusters with high coordination numbers, nine-coordination being particularly important in the structure of *f*-block elements[22].

FE-SEM analysis was performed in order to determine the particle morphology in detail. Figures 3(a-f) present FE-SEM images of the $Gd(OH)_3$, GdOOH and Gd_2O_3 nanorods. We can see that the as-prepared $Gd(OH)_3$ sample consists of particles with undefined shape (Figure 3(a)). On the other hand, the $Gd(OH)_3$ precursor treated by the MAH method exhibits a controlled and well-defined morphology, where nanorods prevail (Figure 3(b)). Similarly, GdOOH and Gd_2O_3 also exhibit a nanorods-like morphology, even after subsequent thermal treatment (Figures 3(b-f)).

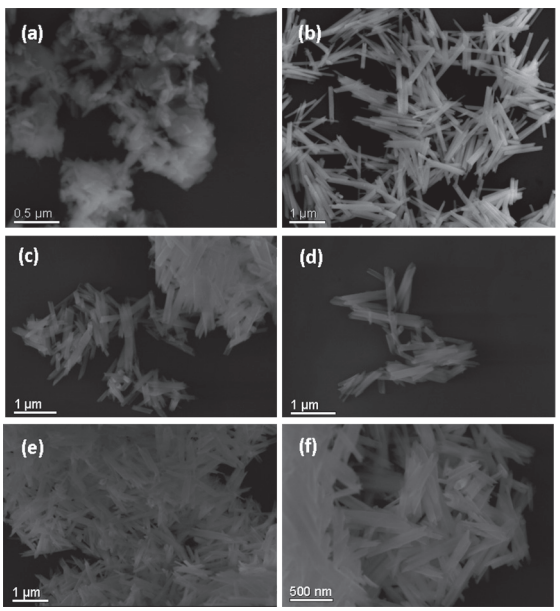

Figure 3: FE-SEM images of (a) as-prepared $Gd(OH)_3$ without the MAH treatment (b) $Gd(OH)_3$ (c-d) GdOOH and (e-f) Gd_2O_3 nanorods.

It can be seen that $Gd(OH)_3$ nanorods (Figure 3(b)) have a narrow size distribution with an average length of about 0.9 µm and diameter of about 12.4 nm, respectively. Figures 3 (c-d) exhibit the same morphology for the intermediate GdOOH compound formed with the thermal treatment at 380 ºC. There was no morphological change after the calcination process, indicating a stability of the nanorods obtained. However, there was a reduction in the size of the

nanorods (average length of about 0.64 µm and diameter of about 14.3 nm), confirming the crystallite size results presented earlier. Moreover, similar results were found for the Gd_2O_3 nanorods (Figures 3(e-f)) formed after the thermal treatment at 600 ºC, in which a reduction of the nanorods size (average length of about 0.60 µm and diameter of about 13.2 nm) was also observed.

Then, we can verify that the synthetic strategy employed in this study allows the preparation of materials with high purity and well-defined morphologies at low temperatures and short synthesis times. Successful conditions for this synthesis using the MAH method are attributed to the rapid and effective interaction between the electromagnetic radiation and the permanent dipole moment of water molecules[23,24]. The permanent dipoles of water are induced in solution and can produce a rapid heating of the system because they interact directly with microwaves. This kind of interaction is directly related to the water capacity for electromagnetic radiation absorption and efficiency in converting electromagnetic radiation to thermal energy[25-28]. Therefore, the reaction time and temperature necessary for obtaining of such materials in this work is significantly lower than those described in the literature[29-32] providing a significant improvement on crystallinity and morphology.

In this work, the Kubelka-Munk method was employed to calculate the E_g values. The direct E_g values were found to be 5.56, 5.12 and 5.04 eV for the $Gd(OH)_3$, GdOOH and Gd_2O_3 nanorods, respectively (Figures 4 (a)). These values agree with those reported in the literature as compared to bulk band gap values[33,34]. Some small variations are attributed to the fact that the E_g values depend on the method of preparation and the experimental conditions like the type of surfactant, temperature and processing time. These key factors can favor or inhibit the formation of structural defects, which can control the degree of structural order-disorder of the material and consequently, the number of intermediate energy levels within the band gap[35].

However, it has been revealed that the E_g values are strongly dependent on the crystalline structure, and are very sensitive to the effects of the structural order-disorder, as well as the conditions of synthesis used in the preparation of these complex functional materials. The crystal growth process reported in this study might lead to both surface and bulk modifications due to structural changes, which are directly linked to the appearance of new intermediary energy levels within the forbidden band gap[36]. This has a major impact on the physical and chemical properties of the nanorods, namely over its PL emission behavior (Figure 4(d)).

PL emission spectra of the $Gd(OH)_3$, GdOOH and Gd_2O_3 nanorods, excited at 350 nm are shown in Figure 4(b). All the samples exhibit a broad emission band at room temperature, typical of a multiphonon process. As shown in Figure 4(b), the PL emission with a maximum at 508 nm corresponds to the $Gd(OH)_3$ phase, while the other two peaks with lower

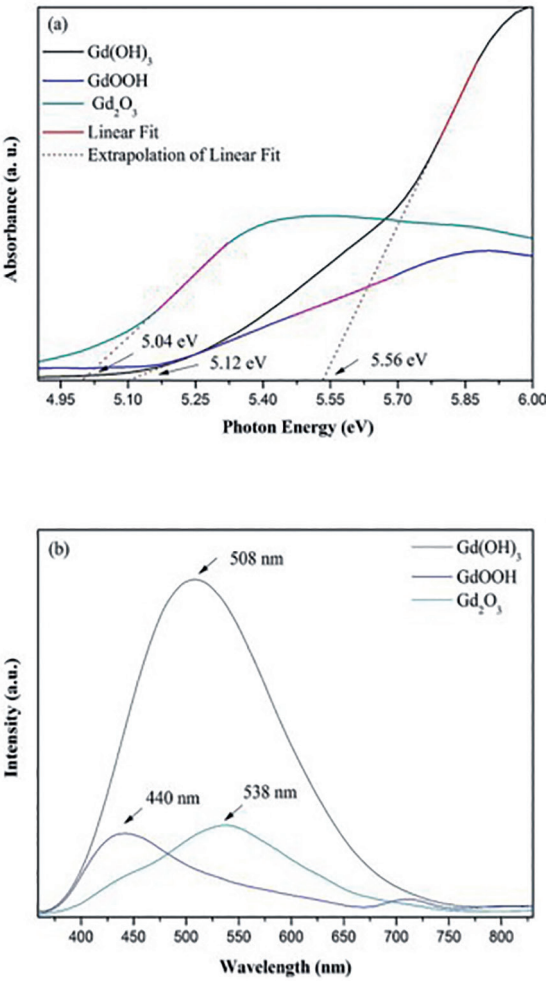

Figure 4: (a) Diffuse reflectance spectra of nanorods and (b) PL at room temperature.

intensities centered at 440 and 538 nm are ascribed to the PL emissions of GdOOH and Gd_2O_3, respectively. Essentially, Gd^{3+} has a simpler emission spectrum in comparison to the other trivalent rare-earth ions[29]. However, we observe a green shift effect on the emission spectrum (Figure 4b) when we compare the conversion of $Gd(OH)_3$ on Gd_2O_3. These emissions are attributed to different types of surface defects of Schottky and Frenkel types[35]. According to Wang's proposal[37], the green emission band may attribute to the recombination of a delocalized electron close to the conduction band with a single charged state of surface oxygen vacancy. In oxide systems, typically oxygen vacancies are prevalent and the presence of such defects contribute significantly to the modified photoluminescence response[37].

However, different density of oxygen vacancies might arouse differences of PL intensities as shown in emission pattern of Figure 4 (b). The PL emission can be a probe for the structural evaluation of materials[9,36,38]. Therefore, direct observation of oxygen vacancies is difficult, but spectroscopic

studies can provide indirect evidences in support of them. More information about the nature of these defects may be elucidated in a future study, using quantum mechanical calculations and experimental techniques such as electron paramagnetic resonance (EPR), X-ray photoelectron spectroscopy (XPS), and X-ray absorption near-edge spectroscopy (XANES). Zhang and co-authors[39] have demonstrated that luminescence results can be employed as a simple probe for oxygen vacancies in TiO_2 nanoparticles. In another work, studies of visible luminescence in TiO_2 nanotubes and EPR spectrum provide strong evidence characteristic of single-electron-trapped oxygen vacancies[40].

Indeed, it is well known that the crystal structure depends on the experimental conditions such as heat treatment, which may cause changes to its electronic structure, and thus, has an important role in the PL profile[9]. We can observe that the $Gd(OH)_3$ compound presents the most intense PL emission (Fig 4b). This effect can be attributed to defects that cause structural disorder yielding intermediate levels in the band gap, which is essential for the PL phenomenon. An improved structural organization has been achieved with further thermal treatment during the annealing process. The resulting GdOOH and Gd_2O_3 compounds present lower PL intensities. These results corroborate with those obtained by UV measurements [Figure 4 (a)]. As shown before, the band gap values of the GdOOH and Gd_2O_3 samples were lower than those presented by $Gd(OH)_3$. Studies on intermediate levels in band gap and structural order-disorder showed a decrease in the optical band gap according to the structural organization[41]. Our group has postulated that the PL intensity in inorganic oxides is also associated with the thermal treatment history, structural order-disorder, and electronic levels in the band gap[41,14].

Figure 5 shows the Commission Internationale de L'Eclairage (CIE) diagram for the compounds with respective assignment of their colors. Specifically, the CIE chromaticity coordinates [x-axis, y-axis] are [x = 0.2801, y = 0.4052], [x = 0.2608, y = 0.2527], and [x = 0.3455, y = 0.4277] corresponding to emission color coordinates for the $Gd(OH)_3$, GdOOH and Gd_2O_3, respectively. These results clearly demonstrate the green shift effect and corroborate the observed PL behavior.

Moreover, an earlier study has demonstrated the synthesis of rare-earth doped Gd_2O_3 nanoparticles[42]. Multicolor emissions at selected wavelengths could be obtained by altering the doping concentration in the triple-doped sample. Based on the CIE coordinates, it could be inferred that double-doped Gd_2O_3 with the composition Tb = 0.05% and Dy = 1.95 mol%, when excited at 247 nm, emits white light, which is closest to the standard noon daylight. Hence, it can be inferred that by altering the doping content of the rare-earth ions in a suitable host lattice like Gd_2O_3, it is possible to achieve desired emission colors.

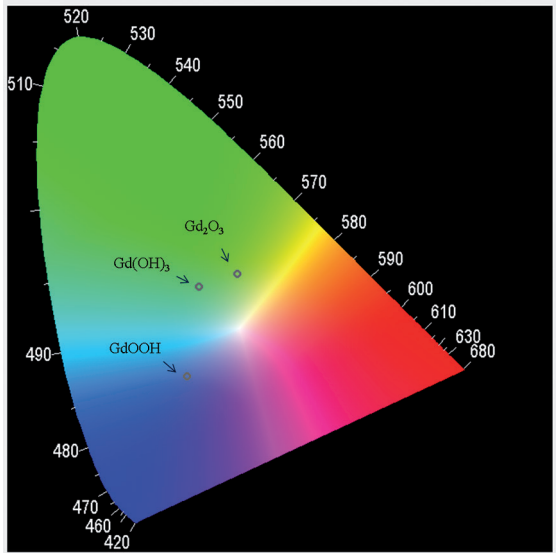

Figure 5: CIE chromaticity diagram for the nanorods.

4. Conclusions

In summary, the method employed is simple and fast to obtain highly crystalline nanorods-like oxides and with unique morphology once the reaction time necessary for the synthesis of such materials is significantly lower than that used in the most previous works. The results contribute to an insight of the crystal structure and chemical composition and its impact the on the optical properties of the $Gd(OH)_3$, GdOOH and Gd_2O_3 obtained. So, shape, size, interaction between particles and synthesis technique play an important role for optical behavior of the studied oxides. Therefore, such properties enable the potential application of these complex functional materials as high-quality phosphors and optoelectronics devices.

5. Acknowledgments

The authors acknowledge the support of the Brazilian agencies FAPESP-CDMF: 2013/07296-2, FAPESP 2013/07437-5, CAPES/PROCAD: 182441, CNPq: 554580/2010-1, CNPq: 485518/2013-9 and FAPEG. Special thanks by INTMF and LabMic/UFG.

6. References

1. Wang X, Sun XM, Yu D, Zou BS, Li Y. Rare earth compound nanotubes. *Advanced Materials*. 2003;15(17):1442-1445.

2. Wang X, Li Y. Rare-earth-compound nanowires, nanotubes, and fullerene-like nanoparticles: Synthesis, characterization, and properties. *Chemistry - A European Journal*. 2003;9(22):5627-5635.

3. Cheraghali R, Aghazadeh M. A Simple and Facile Electrochemical Route to Synthesis of Metal Hydroxides and Oxides Ultrafine Nanoparticles (M=La, Gd, Ni and Co). *Analytical & Bioanalytical Electrochemistry*. 2016;8(1):64-77.

4. Majeed S, Shivashankar SA. Microspherical, hierarchical structures of blue-green-emitting Dy:GdOOH and Dy:Gd_2O_3. *Materials Letters*. 2014;125:136-139.

5. Panda AB, Glaspell G, El-Shall MS. Microwave synthesis and optical properties of uniform nanorods and nanoplates of rare earth oxides. *The Journal of Physical Chemistry C*. 2007;111(5):1861-1864.

6. Xiao H, Li P, Jia F, Zhang L. General nonaqueous sol-gel synthesis of nanostructured Sm_2O_3, Gd_2O_3, Dy_2O_3, and Gd_2O_3:Eu^{3+} phosphor. *The Journal of Physical Chemistry C*. 2009;113(50):21034-21041.

7. Tamrakar RK, Bisen DP, Brahme N. Comparison of photoluminescence properties of Gd_2O_3 phosphor synthesized by combustion and solid state reaction method. *Journal of Radiation Research and Applied* Sciences. 2014;7(4):550-559.

8. Bedekar V, Dutta DP, Tyagi AK. White light emission from spin coated Gd_2O_3:Dy nano phosphors synthesized using polyol technique. *Journal of Nanoscience and Nanotechnology*. 2010;10(12):8234-8238.

9. La Porta FA, Andrés J, Li MS, Sambrano JR, Varela JA, Longo E. Zinc blende *versus* wurtzite ZnS nanoparticles: control of the phase and optical properties by tetrabutylammonium hydroxide. *Physical Chemistry Chemical Physics*. 2014;16(37):20127-20137.

10. Ribeiro PC, Costa ACFM, Kiminami RHGA, Sasaki JM, Lira HL. Synthesis of TiO_2 by the Pechini method and photocatalytic degradation of methyl red. *Materials Research*. 2013;16(2):468-472.

11. Garcia-Contreras R, Scougall-Vilchis RJ, Contreras-Bulnes R, Sakagami H, Morales-Luckie RA, Nakajima H. Mechanical, antibacterial and bond strength properties of nano-titanium-enriched glass ionomer cement. *Journal of Applied Oral Science.* 2015;23(3):321-328.

12. Gonçalves RF, Godinho MJ, Marques APA, Santos MRC, Rosa ILV, Longo E, et al. Structure, morphology, and optical properties of $(Ca_{1-3x}\ Eu_{2x})WO_4$ microcrystals. *Electronic Materials Letters*. 2015;11(2):193-197.

13. Prabaharan DMDM, Sadaiyandi K, Mahendran M, Sagadevan S. Structural, Optical, Morphological and Dielectric Properties of Cerium Oxide Nanoparticles. *Materials Research*. 2016;19(2):478-482.

14. Gonçalves RF, Lima ARF, Godinho MJ, Moura AP, Espinosa J, Longo E, et al. Synthesis of Pr^{3+}-doped $CaTiO_3$ using polymeric precursor and microwave-assisted hydrothermal methods: a comparative study. *Ceramics International*. 2015;41(10 Part A):12841-12848.

15. Chang C, Zhang Q, Mao D. The hydrothermal preparation, crystal structure and photoluminescent properties of GdOOH nanorods. *Nanotechnology*. 2006;17(8):1981-1993.

16. Jia G, Liu K, Zheng Y, Song Y, Yang M, You HP. Highly uniform $Gd(OH)_3$ and Gd_2O_3:Eu^{3+} nanotubes: Facile synthesis and luminescence properties. *The Journal of Physical Chemistry C.* 2009;113(15):6050-6055.

17. Guinier A. *X-Ray Diffraction in Crystals, Imperfect Crystals, and Amorphous Bodi*es. San Francisco: W. H. Freeman; 1963.

18. Le Luyer C, García-Murillo A, Bernstein E, Mugnier J. Waveguide Raman spectroscopy of sol–gel Gd_2O_3 thin films. *Journal of Raman Spectroscopy*. 2003;34(3):234-239.

19. Majeed S, Shivashankar SA. Novel spherical hierarchical structures of GdOOH and Eu:GdOOH: rapid microwave-assisted synthesis through self-assembly, thermal conversion to oxides, and optical studies. *Journal of Materials Chemistry C*. 2014;2(16):2965-2974.

20. Zhang CC, Zhang ZM, Dai RC, Wang ZP, Ding ZJ. High Pressure Luminescence and Raman Studies on the Phase Transition of Gd_2O_3:Eu^{3+} Nanorods. *Journal of Nanoscience and Nanotechnology*. 2011;11(11):9887-9891.

21. Momma K, Izumi F. VESTA 3 for three-dimensional visualization of crystal, volumetric and morphology data. *Journal of Applied Crystallography*. 2011;44:1272-1276.

22. Shriver DF, Atkins PW, Overton TL, Rourke JP, Weller MT, Armstrong FA. Shriver & Atkins Inorganic Chemistry. New York: W. H. Freeman; 2006. 848 p.

23. Dalmaschio CJ, Ribeiro C, Leite ER. Impact of the colloidal state on the oriented attachment growth mechanism. *Nanoscale*. 2010;2(11):2336-2345.

24. Godinho M, Ribeiro C, Longo E, Leite ER. Influence of microwave heating on the growth of gadolinium-doped cerium oxide nanorods. *Crystal Growth & Design*. 2008;8(2):384-386.

25. Lee EJH, Ribeiro C, Longo E, Leite ER. Oriented attachment: An effective mechanism in the formation of anisotropic nanocrystals. *The Journal of Physical Chemistry B*. 2005;109(44):20842-20846.

26. Li C, Liu H, Yang J. A facile hydrothermal approach to the synthesis of nanoscale rare earth hydroxides. *Nanoelcale Research Letters*. 2015;10:144.

27. Seo S, Yang H, Holloway PH. Controlled shape growth of Eu- or Tb-doped luminescent Gd_2O_3 colloidal nanocrystals. *Journal of Colloid and Interface Science*. 2009;331(1):236-242.

28. Gonçalves RF, Moura AP, Godinho MJ, Longo E, Machado MAC, de Castro DA, et al. Crystal growth and photoluminescence of europium-doped strontium titanate prepared by a microwave hydrothermal method. *Ceramics International*. 2015;41(3A):3549-3554.

29. Hazarika S, Paul N, Mohanta D. Rapid hydrothermal route to synthesize cubic-phase gadolinium oxide nanorods. *Bulletin of Materials Science*. 2014;37(4):789-796.

30. Kang JG, Min BK, Sohn Y. Synthesis and characterization of $Gd(OH)_3$ and $Gd2O_3$ nanorods. *Ceramics International*. 2015;41(1B):1243-1248.

31. Dhananjaya N, Nagabhushana H, Nagabhushana BM, Rudraswamy B, Shivakumara C, Chakradhar RPS. Hydrothermal synthesis, characterization and Raman studies of Eu^{3+} activated Gd_2O_3 nanorods. *Physica B: Condensed Matter*. 2011;406(9):1639-1644.

32. Li S, Li Q, Wang K, Zhou M, Huang X, Liu J, et al. Pressure-induced irreversible phase transition in the energetic material urea nitrate: combined Raman scattering and X-ray diffraction study. *The Journal of Physical Chemistry C*. 2013;117(1):152-159.

33. Chen F, Zhang XH, Hu XD, Zhang W, Zeng R, Liu PD, et al. Synthesis and characteristics of nanorods of gadolinium hydroxide and gadolinium oxide. *Journal of Alloys and Compounds*. 2016;664:311-316.

34. Sahoo NK, Thakur S, Senthikumar M, Bhattacharyya D, Das NC. Reactive electron beam evaporation of gadolinium oxide optical thin films for ultraviolet and deep ultraviolet laser wavelengths. *Thin Solid Films*. 2005;440(1-2):155-168.

35. Dhananjaya N, Nagabhushana H, Nagabhushana BM, Rudraswamy B, Sharma SC, Sunitha DV, et al. Effect of different fuels on structural, thermo and photoluminescent properties of Gd_2O_3 nanoparticles. *Spectrochimica Acta Part A: Molecular and Biomolecular Spectroscopy*. 2012;96:532-540.

36. Silva Junior E, La Porta FA, Liu MS, Andrés J, Varela JA, Longo E. A relationship between structural and electronic order-disorder effects and optical properties in crystalline TiO_2 nanomaterials. *Dalton Transactions (Cambridge, England: 2003)*. 2015;44(7):3159-3175.

37. Hu CG, Liu H, Dong WT, Zhang YY, Bao G, Lao CS, et al. $La(OH)_3$ and La_2O_3 Nanobelts-Synthesis and Physical Properties. *Advanced Materials*. 2007;19(3):470-474.

38. Longo VM, Cavalcante LS, Paris EC, Sczancoski JC, Pizani PS, Li MS, et al. Hierarchical assembly of $CaMoO_4$ nano-octahedrons and their photoluminescence properties. *The Journal of Physical Chemistry C*. 2011;115(13):5207-5219.

39. Zhang L, Wang S, Lu C. Detection of Oxygen Vacancies in Oxides by Defect-Dependent Cataluminescence. *Analytical Chemistry.* 2015;87(14):7313-7320.

40. Qian L, Jin ZS, Zhang JW, Huang YB, Zhang ZJ, Du ZL. Study of the visible-excitation luminescence of NTA-TiO_2(AB) with single-electron-trapped oxygen vacancies. *Applied Physics A: Materials Science & Processing*. 2005;80(8):1801-1805.

41. Milanez J, de Figueiredo AT, de Lazaro S, Longo VM, Erlo R, Mastelaro VR, et al. The role of oxygen vacancy in the photoluminescence property at room temperature of the $CaTiO_3$. *Journal of Applied Physics*. 2009;106(4):043526.

42. Bedekar V, Dutta DP, Mohapatra M, Godbole SV, Ghildiyal R, Tyagi AK. Rare-earth doped gadolinia based phosphors for potential multicolor and white light emitting deep UV LEDs. *Nanotechnology*. 2009;20(12):125707.